Phase space localization and matrix element distributions in systems with mixed classical phase space

Bernhard Mehlig,[1,2] Kirsten Müller,[3] and Bruno Eckhardt[4]
[1]*Isaac Newton Institute for Mathematical Sciences, 20 Clarkson Road, Cambridge CB3 0EH, United Kingdom*
[2]*Theoretical Physics, University of Oxford, 1 Keble Road, Oxford OX1 3NP, United Kingdom*
[3]*Institut für Physik, Technische Universität Chemnitz, D-09107 Chemnitz, Germany*
[4]*Fachbereich Physik, Philipps Universität Marburg, D-35032 Marburg, Germany*
(Received 11 November 1998)

We consider distributions of diagonal matrix elements for smooth observables in systems whose classical phase space has a mixture of chaotic and nearly integrable regions. The quantum distributions agree very well with distributions obtained from classical trajectory segments whose length is the Heisenberg time. Non-Gaussian wings in the distributions can be linked to classical trapping in certain parts of phase space, sometimes connected to islands, but also to regions separated by other barriers to transport. Thus classical deviations from ergodicity are quantitatively reflected in quantum matrix elements. The relation to scars is discussed. [S1063-651X(99)04205-1]

PACS number(s): 05.45.−a, 03.65.+Sq

I. INTRODUCTION

High-lying quantum states in many systems such as atoms, molecules, nuclei, and mesoscopic solids show fluctuations in energy-level spacings and matrix elements which can very accurately be modeled by statistical ensembles. These fluctuations are universal in that they can be described by random-matrix theory [1–4]. A connection to classical chaos can be established in the case of rapidly decaying correlations and classical ergodicity [5–7]. However, in most systems, including the stadium billiard [8], dynamic correlations may persist for long times and the rate of exploration for some regions in phase space is very slow. Such inhomogeneities in classical phase space can be due to adiabatic separation of time scales [9–11], cantori [12] or other barriers to transport. There are indications that some quantum effects can be related to this classical behavior. We mention diffusion through cantori [13], random matrix models for coupled regions [14], or the close relationship between classical diffusion and quantum localization noted in [15].

In the present article we study fluctuations of expectation values of operators with a smooth classical limit. It is assumed that the operator $\hat{A}$ does not commute with the Hamilton operator $\hat{H}$. Such fluctuations are of considerable interest since they are directly related to Franck-Condon factors and other experimentally accessible quantities. As shown in [16], for hyperbolic systems they can also be related to classical fluctuations. One can thus expect that inhomogeneities or correlations in the classical dynamics should also be reflected in these fluctuations. It is precisely these effects we would like to identify and demonstrate here.

In classically hyperbolic quantum systems, fluctuations of expectation values are universal: they are Gaussian as predicted by random-matrix theory [19]. The corresponding mean μ_{diag} and variance σ^2_{diag} are nonuniversal parameters and depend on the observable considered. Both can be estimated semiclassically. For the mean value a semiclassical estimate is given by the phase-space average of the observable in question. The variance was studied in [16] where it was shown that it decays as T_{H}^{-1}, where $T_{\mathrm{H}}=2\pi\hbar/\Delta(E)$ is the Heisenberg time [$\Delta(E)$ is the mean level spacing at energy E]. This implies that fluctuations of expectation values can be modeled by the fluctuation properties of classical averages along trajectory segments of length T_{H}. It is intuitively appealing that this is roughly the time beyond which classical and quantum time evolutions depart. By way of two examples, the quantized baker's map and hydrogen in a magnetic field, it was shown that not only the mean and the variance but also the full quantum distributions of expectation values were very well modeled by the corresponding classical distribution functions (see [17,18] for further examples).

The fluctuation properties of expectation values in systems where the classical dynamics is dominated by phase-space inhomogeneities can be very different and nonuniversal, as we show in the following. It is then natural to ask to which extent fluctuations of expectation values in such systems can be characterized in terms of the classical dynamics. That this should be possible is suggested by the following qualitative argument: Phase-space regions characterized by smaller than average classical instability may trap classical trajectories. At the same time, such regions give rise to wave-function localization. Such localized wave functions might give matrix elements far from the ergodic mean and might be noticeable in the distribution. As it turns out, this picture gives a remarkably accurate description of the distribution.

A quantitative theoretical characterization of fluctuations of expectation values in systems with mixed classical dynamics is still missing as the analysis of [16] does not immediately apply there. The assumptions about the distribution of classical trajectory segments, for example, fail badly in the integrable islands. However, we here present qualitative arguments and numerical examples to support the following observations which are natural extrapolations of the work on hyperbolic systems. First, the presence of integrable

islands substantially alters the distribution of expectation values: it retains a finite width even as the Heisenberg time diverges. Second, matrix element distributions in systems with mixed phase space can to a good approximation be described as a superposition of the two distributions, one for the integrable part and one for the hyperbolic part. Third, the inhomogeneities in systems with mixed phase space, in particular due to the infinite hierarchy of islands around islands or due to cantori affect the distributions of classical trajectory segments and are also reflected in the distribution of quantum expectation values. This suggests that individual wave functions also show a larger than average amplitude in these regions, an effect reminiscent of scarring [20,21].

Our numerical support is based on two quite different systems exhibiting a mixed phase space. The first one, studied in Sec. II, is a planar billiard system whose boundary is given by $r=1+a\cos\phi$ (in polar coordinates r and ϕ) [22]. As a second example we consider in Sec. III the hydrogen atom in a strong magnetic field [23]. In both cases we find close similarities between classical and quantum behaviors in regions of mixed phase space. Moreover, we observe strong deviations from Gaussian distributions, in marked difference to what might be expected from random-matrix theory.

II. A NONHYPERBOLIC BILLIARD

We begin by discussing our results for the family of billiards. For $a=0$, the billiard is a circular disk with integrable classical dynamics. For $a=1$, on the other hand, the boundary has a cusp and the billiard is the fully hyperbolic cardioid billiard [22]. The quantum eigenvalues E_n and the eigenfunctions $\psi_n(x,y)$ are determined from the Helmholtz equation $[\Delta - z_n^2]\psi_n(x,y)=0$ with Dirichlet boundary conditions, and $\hbar z_n=\sqrt{2mE_n}$. We have calculated matrix elements $\langle\psi_n|\hat{A}|\psi_n\rangle$ of the observable $A(\boldsymbol{p},\boldsymbol{q})=|\boldsymbol{q}|^2$, where $\boldsymbol{p}$ and $\boldsymbol{q}=(x,y)$ are phase-space coordinates. The corresponding distribution functions are shown in Fig. 1(a) for the integrable case $a=0$ and in Fig. 1(b) for an example with mixed phase space, $a=1/2$.

A. Integrable case

In the integrable case, $a=0$, the Wigner functions of the eigenstates $|\boldsymbol{n}\rangle$ are uniformly distributed over the corresponding quantizing tori $\boldsymbol{I}=(\boldsymbol{n}+\boldsymbol{l})\hbar$. The matrix elements can be approximated, to order $O(\hbar^2)$, by the averages of the phase-space observable A over the quantizing tori, $A_0(\boldsymbol{I})=(2\pi)^{-1}\int d^2\theta A(\boldsymbol{I},\boldsymbol{\theta})$. Here $(\boldsymbol{I},\boldsymbol{\theta})$ are action and angle variables. This allows us to obtain a semiclassical expression for the distribution function of diagonal matrix elements,

$$P(A)=\int d\mu(\boldsymbol{I})\,\delta[A-A_0(\boldsymbol{I})], \tag{1}$$

where $d\mu(\boldsymbol{I})=\Delta(E)d^2I\,\delta[E-H(\boldsymbol{I})]$ is the invariant measure on the tori. For the variance one obtains

$$\sigma^2_{\mathrm{diag}}=\int d\mu(\boldsymbol{I})|A_0(\boldsymbol{I})|^2-\left|\int d\mu(\boldsymbol{I})A_0(\boldsymbol{I})\right|^2. \tag{2}$$

$A_0(\boldsymbol{I})$ may be obtained as a trajectory average of $A(\boldsymbol{I},\boldsymbol{\theta})$ over the torus for sufficiently large T (where T is the time along the trajectory). The right-hand side of Eq. (2) is independent of T and thus the quantum variance does not narrow as $\hbar\to 0$, as opposed to the hyperbolic case, where in systems with two degrees of freedom $\sigma^2_{\mathrm{diag}}\sim T_{\mathrm{H}}^{-1}\sim\hbar$.

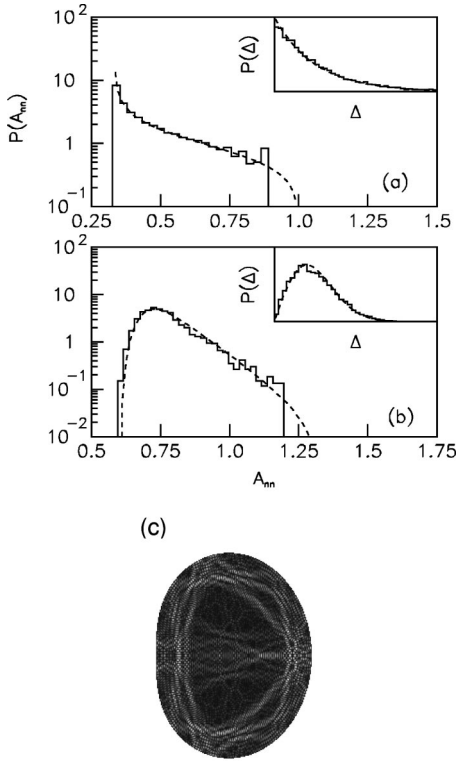

FIG. 1. (a) The distribution of matrix elements for the billiard with deformation parameter $a=0$ (full line). The dashed line shows the corresponding classical distribution function [see Eq. (1)]. The inset shows the histogram of the nearest-neighbor level spacings. The Poisson distribution is shown as a dashed line. (b) Same but for $a=0.5$. The dashed line shows the distribution function of $T_{\mathrm{H}}^{-1}\int_0^{T_{\mathrm{H}}}dtA(\boldsymbol{p}_t,\boldsymbol{q}_t)$. (c) Wave function exhibiting the localization properties discussed in the text.

For the distribution function of the observable $A(\boldsymbol{p},\boldsymbol{q})=|\boldsymbol{q}|^2$ in the circle we obtain

$$P(A)=3/\pi[(1-A)/(A-1/3)]^{1/2}.$$

This result is also shown in Fig. 1(a) and compares very well with the distribution of matrix elements. Note that while the nearest-neighbor level separation shows universal behavior [inset of Fig. 1(a)], the distribution function $P(A)$ does not. Since elliptic islands in systems with mixed phase space can be described by approximate action and angle variables, their contribution to the matrix element distribution can be calculated from Eq. (1) and will be nonuniversal (see below).

B. Mixed case

For $a=1/2$ the classical motion is largely ergodic [24]. However, there are elliptic islands on tiny scales and they influence the classical dynamics and the correlations. As they are too small to support quantum states for the value of Planck's constant we consider, they do not influence some measures of quantum chaos. For instance, the distribution of nearest-neighbor level spacings is in good agreement with

the Wigner surmise $P(\Delta)=\pi/2\Delta\exp(-\pi\Delta^2/4)$, as shown in the inset of Fig. 1(b). However, the rate of exploration of phase space is highly nonuniform and this effects the distribution function of classical averages $T_p^{-1}\int_0^{T_p}dtA(\boldsymbol{p}_t,\boldsymbol{q}_t)$ of the observable along periodic orbits or classical trajectory segments of length T_p. In Ref. [16] it was argued that the distribution of quantum-mechanical matrix elements reflects the classical distribution function with $T_p\simeq T_{\mathrm{H}}$. Figure 1(b) shows that this is indeed the case. Both distributions exhibit a characteristic shoulder due to the presence of several families of whispering gallery orbits which strongly influence the phase flow. They are all unstable but their Lyapunov exponents increase only logarithmically with the number n of bounces at the perimeter, $\lambda_n\sim a+b\ln n$. These families create comparatively stable regions of phase space where trajectories tend to be trapped, thus contributing to the tails of the classical distribution function. The quantum distribution functions reflect this classical localization. In particular, wave functions corresponding to matrix elements in the shoulder of the distribution are localized in the vicinity of the boundary [compare Fig. 1(c)].

III. THE HYDROGEN ATOM IN A STRONG MAGNETIC FIELD

The second example is the hydrogen atom in a strong magnetic field. As usual, we exploit the scaling relations in the system and the mapping onto an anharmonic oscillator in semiparabolic coordinates [23]. The Hamilton function then becomes in atomic units

$$H=\frac{p_\mu^2+p_\nu^2}{2}-E(\mu^2+\nu^2)+\frac{\gamma^2}{8}(\mu^2\nu^4+\mu^4\nu^2)=2, \quad (3)$$

where γ is the strength of the magnetic field. Rewriting Eq. (3) in terms of scaled coordinates $\tilde{\mu}=\gamma^{1/3}\mu$ and $\tilde{\nu}=\gamma^{1/3}\nu$ it can be shown that the classical Hamiltonian depends only on a combination of energy and field, namely, $\epsilon=E\gamma^{-2/3}$. To facilitate the comparison with classical mechanics, we fix ϵ and solve the Schrödinger equation for $z=\gamma^{-1/3}$. The classical action scales linearly with z, $S=\int\boldsymbol{p}d\boldsymbol{q}=z\tilde{S}$. In scaled units the Heisenberg time is $2\pi/\Delta(z)$.

At the scaled energy of $\varepsilon=-0.2$ the classical dynamics is dominated by a large island in phase space. The island around the stable periodic orbit (PO) perpendicular to the magnetic field occupies about 10% of phase space. In Fig. 2(b) we show matrix elements of both positive and negative z parity for the scaled observable $\tilde{A}=1/2\tilde{r}=z^2/2r$. One can clearly distinguish two types of matrix elements, *regular* and *irregular* ones. The irregular matrix elements are scattered around the classical phase-space average of the ergodic component, while the regular matrix elements are arranged on strings. This arrangement is shown in detail in Fig. 2(c), as a function of z_n^{-1}. Finally, in Fig. 2(a) the corresponding distribution function is shown. The contributions from regular and irregular matrix elements are again clearly distinct and we discuss them separately.

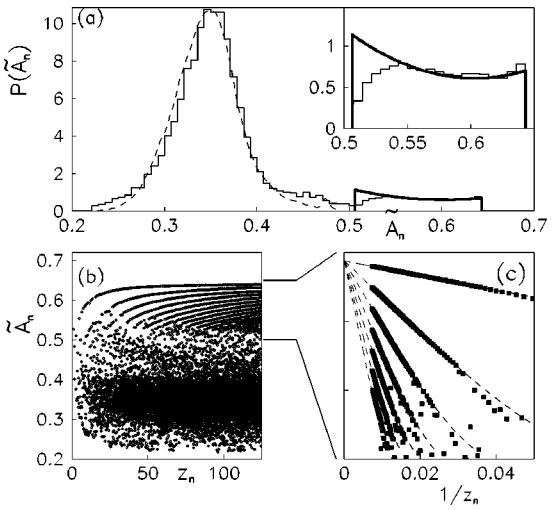

FIG. 2. (a) The distribution of matrix elements $\tilde{A}_{\mathrm{nn}}$ (solid line), the corresponding classical distribution for $2\pi/\Delta(z)\simeq 350$ (dashed line), and the result according to Eq. (1) (heavy line). The inset shows a magnification of the regular contributions. (b) Scaled matrix elements $\tilde{A}_{\mathrm{nn}}=z^2\langle\psi_n|1/2r|\psi_n\rangle$ versus quantum eigenvalues z_n. (c) Regular matrix elements and the semiclassical theory (dashed lines). In all cases, scaled units are used.

A. Regular matrix elements

The chains of eigenvalues in Fig. 2(b) are associated with the elliptic island. The matrix elements can be calculated semiclassically by identifying approximate action and angle variables for the island. Following the method outlined in Ref. [14], we have determined scaled action variables $(\tilde{I}_1,\tilde{I}_2)$. Specifically, we introduce a local coordinate system near the stable PO and define the action $\tilde{I}_2$ corresponding to radial motion in the plane perpendicular to the magnetic field. $\tilde{I}_1$ is chosen corresponding to vibrational motion parallel to the field. For motion along the PO, $\tilde{I}_1=0$ and $\tilde{I}_2=\tilde{S}_p$. In general, $(\tilde{I}_1,\tilde{I}_2)$ are determined numerically. To this end, we consider the Legendre transform $\tilde{J}(\alpha)=\tilde{I}_2+\alpha\tilde{I}_1$, where $\tilde{J}$ denotes the mean action accumulated between two subsequent intersections with the surface-of-section (SOS) and α denotes the winding number of the torus. Again, motion along the PO has $\tilde{J}=\tilde{S}_p$. For rational $\alpha=r/s$ (r, s integer), an orbit closes upon itself after s intersections of the SOS and r turns around the central fixed point. Using 50 approximately periodic trajectories ($s\leqslant 10\,000$) covering the elliptic island, we obtain $\tilde{J}(\alpha)$ as shown in the inset of Fig. 3(a). Both branches of $\tilde{J}(\alpha)$ are fitted using splines (full line). This allows for an accurate calculation of $\tilde{I}_1=d\tilde{J}/d\alpha$ and $\tilde{I}_2=g(\tilde{I}_1)=\tilde{J}-\alpha\tilde{I}_1$ shown in Fig. 3(a) as a full line. The dashed curve shows the result for harmonic approximation of the motion perpendicular to the stable PO, $\tilde{I}_2=\tilde{S}_p-\alpha_p\tilde{I}_1$. Both curves lie close to each other, which explains the success of the quantization scheme by Gutzwiller and Miller [26,27].

The relation $\tilde{I}_2=g(\tilde{I}_1)$ can be checked quantum mechanically by assigning quantum numbers $\boldsymbol{n}=(n_1,n_2)$ to the regu-

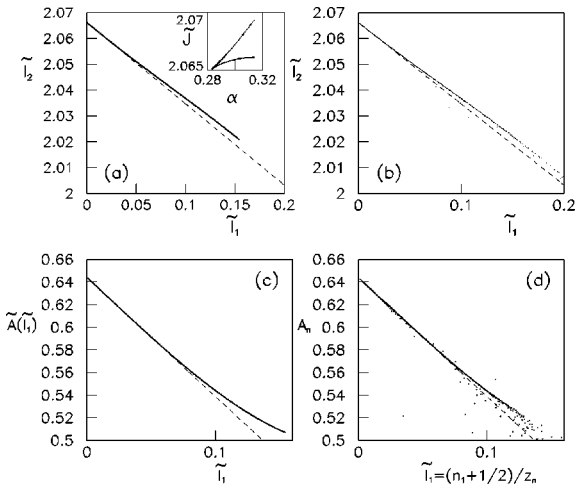

FIG. 3. The relation $\tilde{I}_2=g(\tilde{I}_1)$ between the actions $(\tilde{I}_1,\tilde{I}_2)$, belonging to the regular island, as obtained from classical (a) and quantum (b) calculations. The dashed line corresponds to the harmonic approximation $\tilde{I}_2=\tilde{S}_p-\alpha_p\tilde{I}_1$. The inset of (a) shows the Legendre transform $\tilde{J}(\alpha)=\tilde{I}_2+\alpha\tilde{I}_1$ of the classical curve $\tilde{I}_2=g(\tilde{I}_1)$. (c) The average of the classical phase space observable $\tilde{A}=z^2/2r$ over a given torus as a function of its action $\tilde{I}_1$. (d) The quantum analog shows the exact matrix elements $A_{\boldsymbol{n}}$ as a function of the action of the quantizing tori. The dashed line shows the fit $\tilde{A}_0(\tilde{\boldsymbol{I}})=\tilde{A}_{\rm PO}-\tilde{I}_1$. In all cases, scaled units are used.

lar levels associated with the elliptic island. This is most easily done by inspection of the respective matrix elements $\tilde{A}_{\boldsymbol{n}}$ which fall along lines with fixed quantum number n_1 [cf. Fig. 2(c) with $n_1=0,1,2\ldots$ from top to bottom]. In order to determine n_2, it is sufficient to count the excitations along the PO for one wave function belonging to a particular subgroup $n_1=$const [28].

Making use of the scaling properties, the Einstein-Brillouin-Keller (EBK) quantization conditions may be rewritten as $\tilde{\boldsymbol{I}}=(\boldsymbol{n}+\boldsymbol{l})/z_{\boldsymbol{n}}$, where $(l_2,l_1)=(3/2,1/2)$ denote the Maslov indices of motion parallel and perpendicular to the PO and $z_{\boldsymbol{n}}$ are the exact quantum eigenvalues to which the quantum numbers have been assigned [29]. Figure 3(b) shows the quantized values for (I_2,I_1) obtained in this way. They agree very well with the classical curve. The continuation of the quantum curve beyond the classical border indicates the presence of classical partial barriers such as chains of tiny regular islands near the regular-chaotic surface [14], a point which will be further investigated in connection with the irregular matrix elements below.

By averaging the observable $\tilde{A}$ over the quantizing tori, we obtain semiclassical approximations for individual matrix elements between states associated with the elliptic island. The resulting function $\tilde{A}_0(\tilde{\boldsymbol{I}})$ is shown in Fig. 3(c) as a function of $\tilde{I}_1$. We have $\tilde{A}_0(\tilde{\boldsymbol{I}})\to\tilde{A}_{\rm PO}$ as $\tilde{I}_1\to 0$. A quantum equivalent of Fig. 3(c) is constructed by plotting the exact matrix elements as a function of $\tilde{I}_1=(n_1+1/2)/z_{n_1,n_2}$ [Fig. 3(d)]. Again, the agreement between the quantum and classical curves is very good. For states with small longitudinal quantum number n_2, however, the deviation between exact and semiclassical matrix elements is clearly visible.

The matrix elements and their semiclassical approximations are shown in Fig. 2(c). We observe very good agreement. The matrix elements tend to $\tilde{A}_{\rm PO}$ linearly in $1/z\sim\hbar$ with the gradient given approximately by $n_1+1/2$. In fact, for high energies or small $\tilde{I}_1$ we find $\tilde{A}_0(\tilde{I}_1)\simeq\tilde{A}_{\rm PO}-\tilde{I}_1$ for $\tilde{A}=1/2\tilde{r}$. Together with $\tilde{I}_1=(n_1+1/2)/z$, we obtain $\tilde{A}_{\boldsymbol{n}}\simeq\tilde{A}_{\rm PO}-(n_1+1/2)/z_{\boldsymbol{n}}$ as observed.

It should be noted that Gutzwiller's theory merely predicts that $A_{\boldsymbol{n}}$ approaches $A_{\rm PO}$ as $\hbar$ goes to zero. The approach to the limit, as shown and described in Fig. 2(c), cannot be obtained using Gutzwiller's formula.

Having calculated the regular matrix elements, their distribution function is obtained as follows. To very good accuracy, $\tilde{I}_2\equiv g(\tilde{I}_1)=\tilde{S}_p+\alpha_p\tilde{I}_1$ where $\tilde{S}_p$ and α_p are the scaled action and winding number associated with the PO in the center of the island. This enables us to evaluate the distribution function of regular matrix elements as $P(\tilde{A})=N[\partial\tilde{A}_0(\tilde{\boldsymbol{I}})/\partial\tilde{I}_1]^{-1}$. The normalization N is determined from the fraction of regular phase-space volume. This distribution function is shown in Fig. 2(a) [see also inset of Fig. 2(a)] and agrees well with the quantum-mechanical data except in the vicinity of the border of the island.

B. Irregular matrix elements

The procedure described in the preceeding section allows us to identify and remove the regular matrix elements. What remains is the bulk contribution centered around the microcanonical average $\langle A\rangle_{\rm mc}\simeq 0.349$. This is shown in Fig. 2(a), where we have also plotted the distribution of the averages of $\tilde{A}$ along classical trajectory segments of length [30] of the Heisenberg time $2\pi/\Delta(z)$. As in the case of the billiard, the quantum distribution reflects classical localization in phase space in the same way as the classical distribution does. This is particularly noticeable in the tails of the distributions which show significant deviations from a Gaussian shape.

In order to connect matrix elements and classical phase space structures more quantitatively we project out the states and the trajectories that contribute to certain parts of the quantum and classical distributions, respectively. This is of particular interest in the tails of the distribution, where deviations from Gaussian behavior are strongest. Figure 4 contains a sequence of Poincaré SOS plots. The left panel shows the SOS crossings of all classical trajectory segments that contribute to a specific interval in the observable and the right panel shows typical Husimi distributions of the corresponding quantum states.

The first row in Fig. 4 shows the contributions to the interval $0.45\leqslant\tilde{A}\leqslant 0.5$, in the middle between the island and the chaotic sea. Evidently, all the classical trajectory segments stay close to the vicinity of the island and also the quantum wave functions are localized nearby. Thus the sticking of the classical trajectories near the islands manifests itself in the distribution of average observables and in the quantum wave functions.

If we collect all trajectories with $0.2\leqslant\tilde{A}\leqslant 0.25$ ($\tilde{A}_p=0.2$ for the PO parallel to the magnetic field), their intersections with the SOS appear near the fixed points of the adiabatically stable PO parallel to the magnetic field and the other PO

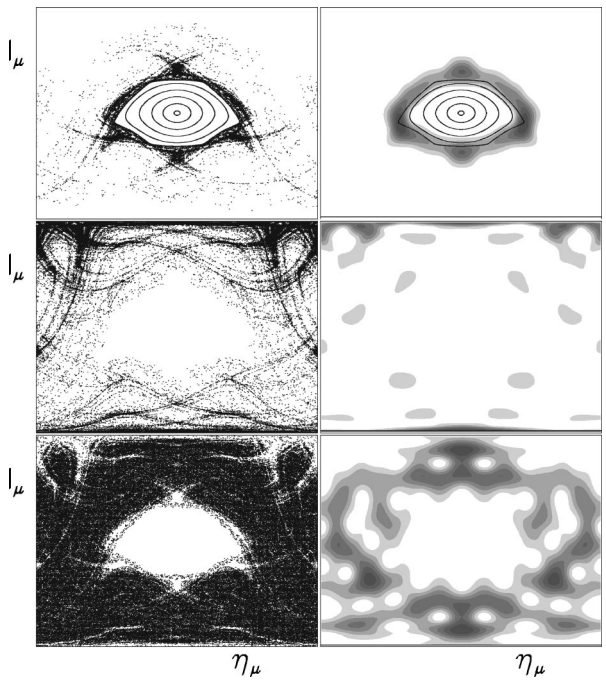

FIG. 4. Plot of the intersection points of classical trajectories (accumulated scaled action $\tilde{S} \simeq 200$) with the SOS (left panel) and Husimi distributions of selected eigenstates (right panel). The trajectories and eigenstates are chosen such that their mean values and matrix elements lie in between certain intervals, namely (0.45,0.5) (first row), (0.2,0.25) (second row), and (0.33,0.37) (third row). For the coordinates on the SOS see [25].

winding around it, as well as near the invariant manifolds of the corresponding fixed points. We also show the Husimi distribution of a corresponding eigenstate, which shows similar localization near the adiabatically stable periodic orbit (Fig. 4, second row).

The third row in Fig. 4 shows the situation for $0.33 \leqslant \tilde{A} \leqslant 0.37$, i.e., in the vicinity of the microcanonical mean. Clearly, the maximum of the irregular distribution(s) is associated with the body of the chaotic phase space, where the less unstable subregions are left out.

Of these findings the ones for the adiabatically stable periodic orbit are particularly interesting since they are not connected to a stable island where the long-time organization due to self-similar structures in phase space is at least qualitatively understood. The effect of the adiabatically stable orbit is to introduce a new time scale in the dynamics combined with a direction of motion with weak instability. Since the comparison between classical and quantum mechanics is based on finite time segments, long time trapping in one region implies that there is less time to explore others and hence a certain lack of ergodicity. For infinite times this deficit will disappear, but for finite times the deviations remain noticeable, and, as Heller has argued, also persist quantum mechanically [31].

IV. CONCLUSIONS

In summary, we have established a close quantum-classical correspondence for distributions of diagonal matrix elements in quantum systems with mixed classical phase space. We have related quantum and classical localization properties and have thus shown how deviations from random-matrix theory in such systems can be understood qualitatively and, to a certain extent, also quantitatively. There remains then the question of the relation between our results and the phenomenon of scars. According to [21] a wave function shows a scar in some region if the quantum probability $|\psi|^2$ is enhanced over the average expected from a uniform microcanonical distribution, perhaps due to a quantum interference effect, similar to weak localization. In the present case, however, the enhancement is purely classical in origin, due to an increased classical trapping time in the localization region (as suggested previously in [10]). Clearly, this phenomenon shows up for finite time segments only and vanishes in the classical limit (where $T_{\mathrm{H}} \to \infty$), a feature it shares with scars in general. Since typical systems have a nonuniform phase space the phenomenon discussed here should be rather widespread and a major source of deviations from random-matrix behavior in matrix elements. However, such an enhancement should be clearly distinguished from scarring due to quantum effects like weak localization. In fact, it is not clear whether scarring without corresponding classical enhancement exists. It would be highly desirable to have a clear-cut example demonstrating this latter type of scarring as opposed to the phenomenon discussed in the present letter.

ACKNOWLEDGMENTS

K.M. gratefully acknowledges support of the SFB 393. B.E. and B.M. would like to thank the Newton Institute, Cambridge, for its hospitality during the completion of this work.

[1] F. Haake, *Quantum Signatures of Classical Chaos* (Springer, Berlin, 1994).
[2] C. E. Porter, *Statistical Theories of Spectra: Fluctuations* (Academic, New York, 1965).
[3] O. Bohigas, in *Chaos and Quantum Physics*, Proceedings of the Les Houches Summer School, Session LII, edited by M.-J. Giannoni, A. Voros, and J. Zinn-Justin (North-Holland, Amsterdam, 1990), p. 87.
[4] A. Müller-Gröhling, T. Guhr, and H. A. Weidenmüller, Phys. Rep. **299**, 190 (1998).
[5] E. B. Bogomolny and J. P. Keating, Phys. Rev. Lett. **77**, 1472 (1996).
[6] A. I. Shnirelman, Usp. Mat. Nauk **29**, 181 (1974).
[7] S. Zelditch, Duke Math. J. **55**, 919 (1987).
[8] F. Vivaldi, G. Casati, and I. Guarneri, Phys. Rev. Lett. **51**, 727 (1983).
[9] B. Eckhardt, G. Hose, and E. Pollak, Phys. Rev. A **39**, 3776 (1989).
[10] B. Eckhardt, J. M. Gomez-Llorente, and E. Pollak, Chem. Phys. Lett. **174**, 325 (1990).

[11] G. Tanner and D. Wintgen, Phys. Rev. Lett. **75**, 2928 (1995).
[12] R. S. Mackay, J. Meiss, and I. C. Percival, Physica D **13**, 55 (1984).
[13] G. Radons, T. Geisel, and J. Rubner, , Adv. Chem. Phys. **1988**, 891 (1988).
[14] O. Bohigas, S. Tomsovic, and D. Ullmo, Phys. Rev. Lett. **64**, 1479 (1990); Phys. Rep. **223**, 45 (1993).
[15] D. Shepelyansky, Phys. Rev. Lett. **56**, 677 (1986).
[16] B. Eckhardt, S. Fishman, J. Keating, O. Agam, J. Main, and K. Müller, Phys. Rev. E **52**, 5893 (1995).
[17] T. O. de Carvalho, J. P. Keating, and J. M. Robbins, J. Phys. A **31**, 5631 (1998).
[18] A. Bäcker, R. Schubert, and P. Stifter, Phys. Rev. E **57**, 5425 (1998); **58**, 5192(E) (1998).
[19] M. Wilkinson, Phys. Rev. A **41**, 4645 (1991).
[20] E. Heller, Phys. Rev. Lett. **53**, 1515 (1984).
[21] E. Heller, *Chaos and Quantum Physics* (North-Holland, Amsterdam, 1991).
[22] M. Robnik, J. Phys. A **16**, 3971 (1983); **17**, 1049 (1983).
[23] H. Friedrich and D. Wintgen, Phys. Rep. **183**, 37 (1989).
[24] A. Hayli, Th. Dumont, J. Moulin-Ollagnier, and J.-M. Strelcyn, J. Phys. A **20**, 3237 (1987).
[25] K. Müller and D. Wintgen, J. Phys. B **27**, 2693 (1994).
[26] D. Wintgen, Phys. Rev. Lett. **61**, 1803 (1988).
[27] W. H. Miller, J. Phys. Chem. **63**, 996 (1975).
[28] Due to the C_4 symmetry of Eq. (3), the stable orbit perpendicular to the field is already periodic after half of its full period; consequently, n_2 takes only even values. States with positive (negative) z parity ($\doteq$ symmetry with respect to $\mu \leftrightarrow \nu$) have even (odd) quantum numbers n_1.
[29] The assignment of quantum numbers may be checked by comparison with the corresponding Gutzwiller eigenvalues $z_{\boldsymbol{n}}^{\mathrm{GW}} = [n_2 + 3/2 + \alpha_p(n_1 + 1/2)]/\tilde{S}_p$, cf. [27].
[30] In the case of the hydrogen atom, T_p is not simply proportional to $\tilde{S}_p$. It can be shown that in the present case periods are to be replaced by scaled actions in semiclassical expressions. Hence, we require trajectory segments satisfying $\tilde{S} = 2\pi/\Delta(z)$. It is still possible to use semiclassical sum rules by appealing to the fact that on average, T_p are proportional to $\tilde{S}_p$.
[31] E. Heller, Phys. Rev. A **35**, 1360 (1987).